Dependence of Second-Harmonic Generation on the Position of the Focus

D. A. KLEINMAN AND R. C. MILLER
Bell Telephone Laboratories, Murray Hill, New Jersey
(Received 3 March 1966)

The theory of second-harmonic generation (SHG) by focused laser beams is compared with experiment in regard to the dependence of the power on the coherence length $[l_c=2\pi/(2k_1-k_2)]$ and position of the focus in the crystal. The treatment neglects absorption and double refraction. The analytical behavior of SHG as a function of focal position is examined by means of an asymptotic representation valid at all positions for the nonmatching case. It is found that SHG should be strongly peaked when the focus is at either of the crystal surfaces. When the coherence length is positive ($2k_1>k_2$) there is an oscillatory fine structure as the focus is moved inside the crystal. There is no fine structure when the focus is moved outside the crystal, or when the coherence length is negative ($2k_1<k_2$). Experiments using the He-Ne gas laser and crystals of $LiNbO_3$ confirm the predictions of the theory. The coherence length in the $LiNbO_3$ could be controlled through the temperature. Satisfactory quantitative agreement was obtained between theory and experiment. A quantitative measurement gave the ratio $d_{33}/d_{31}=6.0\pm1.0$ for $LiNbO_3$ at 1.15 μ.

1. INTRODUCTION

THE properties of second-harmonic generation (SHG) by focused laser beams have recently been described in great detail by Kleinman, Ashkin, and Boyd[1] (KAB). These authors have emphasized the distribution of intensity in the SHG including the asymmetry of the pattern, the sharp edge, and the fine structure. They have also discussed the shift of the pattern which can be produced by a slight change in the index-matching conditions, and have drawn a distinction between nominal matching (the matching of plane waves at the fundamental and harmonic frequencies) and optimum matching (the condition for maximum SHG). Bjorkholm[2] has discussed the conditions for optimum focusing of the laser beam without, however, distinguishing between nominal and optimum matching. Boyd and Kleinman[3] have considered the optimization of SHG with respect to both focus and matching conditions. Prior to this very recent work considerations relevant to SHG by focused beams have been presented by Maker *et al.*,[4] McMahon and Franklin,[5] Francois and Siegman,[6] and Boyd *et al.*[7] In all of these treatments the focused laser beam has been described as a Gaussian beam.[8,1] The excellent agreement between theory and experiment that has been reported[1,2,5–7] indicates that SHG by Gaussian beams is as well understood as SHG by unbounded plane waves.[9–11] As a result it is now possible to make accurate measurements of the nonlinear optical properties of crystals by a variety of methods. Except for dispersion these are the same constants that govern optical parametric amplification,[10,12] and SHG provides the only practical method of measuring these constants at the present time. From this point of view the principal importance of optimization is not to give the experimenter more power for his measurements, but rather to provide him with a technique for establishing a specific experimental condition. It may be expected that the optimum SHG is stationary with respect to small inhomogeneities in the crystal and other small deviations from optimum conditions, and therefore more reliable for quantitative measurements than nonoptimum SHG. Nevertheless, SHG measurements under nonoptimum and nonmatching conditions will continue to be important because matching conditions can only be achieved in relatively few crystals, and even in those crystals only one (or a single linear combination) of the nonlinear coefficients is active under matching conditions.

In this paper we shall describe the behavior of the SHG by focused beams under nonmatching conditions with no double refraction when the position of the focus traverses the crystal. To include double refraction would entail considerable complication. It is significant that detectable SHG can be produced by a gas laser under nonmatching conditions, especially if the beam is focused. In fact, a readily detectable SHG has been observed under nonmatching conditions with a 10-mW He-Ne laser operating in the Gaussian mode at 1.15 μ when focused with a 3-cm focal length lens into a number of piezoelectric crystals. These include quartz, CdS, $BaTiO_3$, $LiNbO_3$, CuCl, and $LiGaO_2$. The SHG is very sensitive to the position of the focus, and the maximum power is not generally produced with the focus in the center of the crystal. The experiments reported here were carried out in single crystals of

[1] D. A. Kleinman, A. Ashkin, and G. D. Boyd, Phys. Rev. **145**, 338 (1966).
[2] J. E. Bjorkholm, Phys. Rev. **142**, 126 (1966).
[3] G. D. Boyd and D. A. Kleinman (to be published).
[4] P. D. Maker, R. W. Terhune, M. Nisenoff, and C. M. Savage, Phys. Rev. Letters **8**, 21 (1962).
[5] D. H. McMahon and A. R. Franklin, Appl. Phys. Letters **6**, 14 (1965).
[6] G. E. Francois and A. E. Siegman, Phys. Rev. **139**, A4 (1965).
[7] G. D. Boyd, A. Ashkin, J. M. Dziedzic, and D. A. Kleinman, Phys. Rev. **137**, A1305 (1965).
[8] G. D. Boyd and J. P. Gordon, Bell System Tech. J. **40**, 489 (1961).
[9] D. A. Kleinman, Phys. Rev. **128**, 1761 (1962).
[10] J. A. Armstrong, N. Bloembergen, J. Ducuing, and P. S. Pershan, Phys. Rev. **127**, 1918 (1962).
[11] N. Bloembergen and P. S. Pershan, Phys. Rev. **128**, 606 (1962).
[12] J. A. Giordmaine and R. C. Miller, Phys. Rev. Letters **14**, 973 (1965).

$LiNbO_3$ [13] with propagation normal to the optic axis, which eliminates double refraction.[14] The matching conditions could be controlled by means of the crystal temperature.[14] The theory necessary for the interpretation of this type of experiment has been given by KAB in terms of a function defined by a definite integral [(7.13) of KAB]:

$$H(\sigma,\kappa,\zeta,\xi)=\frac{1}{2\pi}\int_{-\zeta}^{\xi}\frac{d\tau}{1+i\tau}e^{-\kappa\tau+i\sigma\tau}. \tag{1}$$

The harmonic power in the crystal P_2 is given by [(8.44) of KAB]

$$P_2=(4\pi KP_1^2/\delta_0^2)e^{-2\alpha_1 f-\alpha_2(l-f)}|H|^2, \tag{2}$$

where P_1 is the laser power in the crystal, δ_0 the far-field diffraction half-angle of the laser beam, l the crystal length, f the location of the focus relative to the incident surface, α_1 and α_2 the absorption coefficients for the fundamental and harmonic, respectively, and K contains the nonlinear coefficient of the crystal.[7] For the present case in $LiNbO_3$ this constant is[15]

$$K=[32\pi^2\omega^2/(nc)^3]d_{31}^2, \tag{3}$$

where ω is the second-harmonic angular frequency, n the refractive index, and d_{31} the appropriate nonlinear coefficient in the second-order polarization

$$\mathbf{P}=\mathbf{d}\cdot\mathbf{EE}. \tag{4}$$

The parameters in the function $H(\sigma,\kappa,\zeta,\xi)$ are defined by

$$\sigma=\tfrac{1}{2}b\Delta k=\pi b/l_c, \tag{5}$$

$$\kappa=\tfrac{1}{2}b\alpha=\tfrac{1}{2}b(\alpha_1-\tfrac{1}{2}\alpha_2), \tag{6}$$

$$\zeta=(2/b)f,\quad \xi=(2/b)(l-f). \tag{7}$$

Here b is the confocal parameter[8] of the focus which is related to the diffraction angle δ_0 and minimum spot radius w_0 as follows

$$b=k_1w_0^2=4/k_1\delta_0^2. \tag{8}$$

The neglect of double refraction is valid if $l\ll l_a$, where l_a is the aperture length defined in Ref. 7. The departure from nominal matching is specified by

$$\Delta k=2k_1-k_2, \tag{9}$$

where k_1, k_2 are the propagation constants of plane waves along the laser axis at the fundamental and harmonic frequencies, respectively. The coherence length has been defined[9]

$$l_c=2\pi/\Delta k, \tag{10}$$

which is the distance between successive maxima in the harmonic intensity for SHG by a plane wave k_1. We allow l_c to have either sign corresponding to the sign of Δk.

2. EFFECT OF MISMATCH

A computer program has been developed along the lines outlined in the Appendix of KAB for calculating $|H|^2$. It is useful, however, to have asymptotic approximations in convenient analytical form to describe the important features of the function. It may easily be shown that when $\zeta=\xi$ (focus in the center)

$$\lim_{\xi\to\infty}H(\sigma,0,\xi,\xi)=e^{-\sigma}\theta(\sigma), \tag{11}$$

where $\theta(\sigma)$ is the step function

$$\begin{aligned}\theta(\sigma)&=1, &\sigma>0\\ &=\tfrac{1}{2}, &\sigma=0.\\ &=0, &\sigma<0\end{aligned} \tag{12}$$

We have set $\kappa=0$ since for convenience we shall neglect absorption. It was shown in KAB [Eq. (7.20)] that for

$$\xi\gg1,\quad \zeta\gg1. \tag{13}$$

$H(\sigma,0,\zeta,\xi)$ for all values of σ can be written

$$\begin{aligned}H(\sigma,0,\zeta,\xi)&=e^{-\sigma}\theta(\sigma)-\tfrac{1}{2}[\theta(\sigma)-\theta(-\sigma)]\\ &\quad+\frac{1}{2\pi}[\mathrm{Si}(\sigma\zeta)+i\mathrm{Ci}(\sigma\zeta)+\mathrm{Si}(\sigma\xi)-i\mathrm{Ci}(\sigma\xi)],\end{aligned} \tag{14}$$

where Si and Ci are the sine and cosine integral functions. This gives a continuous representation across the step in (11) at $\sigma=0$, and also shows that H contains oscillatory structure. The structure is revealed most clearly by the asymptotic form [(7.22) of KAB]

$$\begin{aligned}|H(\sigma,0,\zeta,\xi)|^2&=e^{-2\sigma}\theta(\sigma)+\frac{1}{4\pi^2\sigma^2}\left(\frac{1}{\zeta^2}+\frac{1}{\xi^2}\right)-e^{-\sigma}\theta(\sigma)\frac{\cos\sigma\xi}{\pi\sigma\xi}\\ &\quad-e^{-\sigma}\theta(\sigma)\frac{\cos\sigma\zeta}{\pi\sigma\zeta}+\frac{\cos\sigma(\xi+\zeta)}{2\pi\sigma^2\zeta\xi}+\cdots,\end{aligned} \tag{15}$$

valid for large $\sigma\zeta$ and $\sigma\xi$

$$\xi\gg1,\quad \zeta\gg1,\quad |\sigma\xi|>1,\quad |\sigma\zeta|>1. \tag{16}$$

The behavior of $|H(\sigma,0,\xi,\xi)|^2$ as a function of the matching conditions measured by σ is shown in Fig. 1 for $\xi=9.5$. A distinct asymmetry about nominal matching $\sigma=0$ is characteristic of SHG when $\xi\gg1$. Since in this example $\zeta=\xi$, the third and fourth terms of (15) are equal and give rise to a simple fine structure $[-2e^{-\sigma}\cos\sigma\xi]/\pi\sigma\xi$ in the region $0<\sigma<6$. Vertical lines indicate the maxima of $-\cos\sigma\xi$. For $\sigma>8$ and $\sigma<0$ the fine structure is dominated by the last term

[13] K. Nassau, H. J. Levinstein, and G. M. Loiacono, Appl. Phys. Letters **6**, 228 (1965); K. Nassau and H. J. Levinstein, *ibid.* **7**, 69 (1965).

[14] R. C. Miller, G. D. Boyd, and A. Savage, Appl. Phys. Letters **6**, 77 (1965).

[15] G. D. Boyd, R. C. Miller, K. Nassau, W. L. Bond, and A. Savage, Appl. Phys. Letters **5**, 234 (1964).

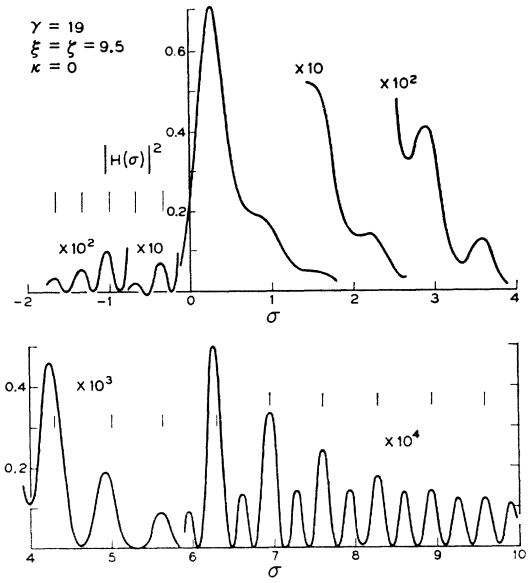

FIG. 1. Second-harmonic power according to (2) as a function of mismatch for parameters shown. Vertical lines at left mark the maxima of $-\cos\sigma\xi$. To show the detail a number of amplified curves are shown.

of (15). The peaks due to this term first appear around $\sigma\sim 6$ as small peaks between the main peaks; with increasing σ the small peaks increase while the larger peaks decrease until they become equal around $\sigma\sim 9$, and then all peaks decrease as required by the last term of (15). The behavior illustrated in Fig. 1 may be described in general as follows: (a) $|H(\sigma,0,\zeta,\xi)|^2$ rises very rapidly with σ near $\sigma=0$ and reaches a maximum at

$$\begin{aligned}\sigma_m &\approx \pi/\xi, \quad \xi<\zeta \\ &\approx \pi/\zeta, \quad \zeta<\xi.\end{aligned} \tag{17}$$

(b) $|H(\sigma)|^2$ is very small for $\sigma<0$ and decays exponentially as $e^{-2\sigma}$ for $\sigma>0$. (c) Superposed on the exponential decay are two oscillatory contributions whose periods depend on the position of the focus. (d) This structure dependent upon the focus extends over the range

$$0<\sigma<\sigma_f, \tag{18}$$

where the limit σ_f is that value of $\sigma>0$ at which additional peaks first appear; from (15) we find that

$$\sigma_f^{-1}\exp(\sigma_f)=2\pi(\xi\zeta)^{1/2}. \tag{19}$$

(e) for $\sigma<0$ and $\sigma>\sigma_f$ the structure becomes independent of the position of the focus; the maxima occur at

$$|\sigma|=2\pi N/(\xi+\zeta) \quad N=\text{positive integer}. \tag{20}$$

From (5), (7), and (10) this may be written as a condition on the crystal length l

$$l=N|l_c|. \tag{21}$$

For comparison we recall[9] that the corresponding condition for SHG by a plane wave k_1 would be

$$l=(N+\tfrac{1}{2})|l_c|. \tag{22}$$

The difference between (21) and (22) is due to the presence of a focus somewhere in the crystal.

3. EFFECT OF MOVING FOCUS

In this paper we are primarily interested in the behavior of $|H|^2$ as a function of ζ, the focal position, when

$$\xi+\zeta=\gamma=2l/b. \tag{23}$$

Therefore it is convenient to replace (1) with the slightly different notation

$$H(\sigma,\kappa,\zeta,\gamma)=\frac{1}{2\pi}\int_{-\zeta}^{\gamma-\zeta}\frac{d\tau}{1+i\tau}e^{-\kappa\tau+i\sigma\tau}. \tag{24}$$

If

$$2\pi H=R+iI, \tag{25}$$

then R and I satisfy the differential equations

$$\frac{\partial R}{\partial\zeta}=\frac{e^{\kappa\zeta}}{1+\zeta^2}[\cos\sigma\zeta+\zeta\sin\sigma\zeta]-\frac{e^{-\kappa(\gamma-\zeta)}}{1+(\gamma-\zeta)^2}\times[\cos\sigma(\gamma-\zeta)+(\gamma-\zeta)\sin\sigma(\gamma-\zeta)], \tag{26}$$

$$\frac{\partial I}{\partial\zeta}=\frac{e^{\kappa\zeta}}{1+\zeta^2}[\zeta\cos\sigma\zeta-\sin\sigma\zeta]+\frac{e^{-\kappa(\gamma-\zeta)}}{1+(\gamma-\zeta)^2}\times[(\gamma-\zeta)\cos\sigma(\gamma-\zeta)-\sin\sigma(\gamma-\zeta)]. \tag{27}$$

The integration of (26) and (27) can be started at any value of ζ at which R and I are known from a previous integration over σ. All numerical integrations will ordinarily start at $\sigma=0$, $\kappa=0$ where

$$\begin{aligned}R(0,0,\zeta,\gamma)&=\tan^{-1}(\gamma-\zeta)+\tan^{-1}\zeta, \\ I(0,0,\zeta,\gamma)&=\ln\left[\frac{1+\zeta^2}{1+(\gamma-\zeta)^2}\right]^{1/2}.\end{aligned} \tag{28}$$

The integrations over σ and κ have been described in the Appendix of KAB. We shall neglect absorption

$$\kappa=0 \tag{29}$$

since this is the case of greatest interest. If the integration of (26), (27) is started at the middle of the crystal $\zeta=\frac{1}{2}\gamma$, one of the initial conditions is

$$I(\sigma,0,\tfrac{1}{2}\gamma,\gamma)\equiv 0. \tag{30}$$

If $|\sigma|$ is sufficiently large an asymptotic expression can be used for the starting value of $R(\sigma,0,\frac{1}{2}\gamma,\gamma)$. It is particularly convenient to start at $\zeta=\frac{1}{2}\gamma$, $I=0$, $R=0$ if values of σ can be chosen at which $|H|^2\approx 0$ according to (15).

The behavior of $|H|^2$ as a function of focal position ζ can be obtained from the asymptotic approximation

(15) providing the conditions (16) for the validity of the approximation are satisfied. We see that $|H|^2$ contains oscillatory terms varying as $\cos\sigma(\gamma-\zeta)$, and $\cos\sigma\zeta$. We see further that this structure is present only when $\sigma>0$. As the focus is brought near the incident surface (ζ decreases) the structure varying as $\cos\sigma\zeta$ increases in amplitude as ζ^{-1}, and a nonoscillatory term increases as ζ^{-2}. This shows that SHG should increase as the focus moves toward the surface when $|\sigma|$ is large enough that (16) can be satisfied over a sizable range of ζ. We can simplify the mathematical description somewhat by considering only one surface, the incident surface, and allowing the other surface to recede to infinity; thus we consider the case

$$\gamma\to\infty\,,\qquad |\sigma|\gg 1. \tag{31}$$

Then (15) becomes

$$|H(\sigma,0,\zeta,\infty)|^2=e^{-2\sigma}\theta(\sigma)+(1/4\pi^2\sigma^2\zeta^2)-e^{-\sigma}\theta(\sigma)(\cos\sigma\zeta/\pi\sigma\zeta)\,, \tag{32}$$

valid when

$$\zeta\gg 1\,,\quad |\sigma\zeta|>1. \tag{33}$$

The distance between consecutive maxima in the SHG as a function of focal position f is given by

$$\sigma\Delta\zeta=2\pi\,, \tag{34}$$

which by (5) and (7) is simply

$$\Delta f=l_c. \tag{35}$$

Thus the coherence length can be determined directly by a distance measurement by moving the focusing lens. It should be noted that Δf is the motion of the focus in the crystal; it is related to the lens motion by

$$\Delta f=n\Delta f(\text{air}). \tag{36}$$

Observation of the structure also gives the sign (positive) of l_c.

In order to discuss the interesting behavior as $\zeta\to 0$ we must obtain a better approximation than (32). It can easily be shown that R and I in (25) can be represented by the integrals ($\kappa=0$)

$$R(\sigma,0,\zeta,\gamma)=e^{-\sigma}\int_{-\infty}^{\sigma}dz\frac{\sin z\zeta+\sin z\xi}{z}e^{z}, \tag{37}$$

$$I(\sigma,0,\zeta,\gamma)=e^{-\sigma}\int_{-\infty}^{\sigma}dz\frac{\cos z\zeta-\cos z\xi}{z}e^{z}, \tag{38}$$

where $\xi=\gamma-\zeta$ according to (23). We introduce the representation

$$(e^z-1)/z=\int_0^1 e^{\beta z}d\beta\,, \tag{39}$$

and write (37) in the form (exact)

$$R=e^{-\sigma}\int_{-\infty}^{\sigma}dz\frac{\sin z\xi}{z}+e^{-\sigma}\int_{-\infty}^{0}dz\frac{\sin z\zeta}{z}+e^{-\sigma}\int_{-\infty}^{\sigma}dz\frac{\sin z\zeta}{z}+e^{-\sigma}\int_0^1 d\beta\int_{-\infty}^{\sigma}dze^{\beta z}\sin z\xi+e^{-\sigma}\int_0^1 d\beta\int_{-\infty}^{\sigma}dze^{\beta z}\sin z\zeta. \tag{40}$$

The integral over z now gives

$$\int_{-\infty}^{\sigma}dz\,e^{\beta z}\sin z\zeta=\frac{e^{\beta\sigma}}{\beta^2+\zeta^2}(\beta\sin\sigma\zeta-\zeta\cos\sigma\zeta)\,, \tag{41}$$

and a similar term in ξ which vanishes as $\xi\to\infty$. The first term of (40) becomes

$$e^{-\sigma}\int_{-\infty}^{\sigma}dz\frac{\sin z\xi}{z}\xrightarrow[\xi\to\infty]{}\pi e^{-\sigma}\theta(\sigma)\,. \tag{42}$$

The second and third terms can be written

$$e^{-\sigma}\int_{-\infty}^{\sigma}dz\frac{\sin z\zeta}{z}=e^{-\sigma}\left[\frac{\pi}{2}\operatorname{sgn}(\zeta)+\operatorname{Si}(\sigma\zeta)\right], \tag{43}$$

where $\operatorname{sgn}(\zeta)=\theta(\zeta)-\theta(-\zeta)$ is the sign of ζ. Thus (40) becomes (exact)

$$R(\sigma,0,\zeta,\infty)=e^{-\sigma}\left[\pi\theta(\sigma)+\frac{\pi}{2}\operatorname{sgn}(\zeta)+\operatorname{Si}(\sigma\zeta)\right]+S(\sigma,\zeta)\sin\sigma\zeta-C(\sigma,\zeta)\cos\sigma\zeta\,, \tag{44}$$

where S and C are the functions

$$S(\sigma,\zeta)=e^{-\sigma}\int_0^1 d\beta\frac{\beta}{\beta^2+\zeta^2}e^{\beta\sigma}\,, \tag{45}$$

$$C(\sigma,\zeta)=e^{-\sigma}\int_0^1 d\beta\frac{\zeta}{\beta^2+\zeta^2}e^{\beta\sigma}. \tag{46}$$

In the same way we obtain the representation (exact)

$$I(\sigma,0,\zeta,\infty)=e^{-\sigma}\operatorname{Ci}(\sigma\zeta)+S(\sigma,\zeta)\cos\sigma\zeta+C(\sigma,\zeta)\sin\sigma\zeta. \tag{47}$$

Since these representations are exact they are continuous functions of ζ; the discontinuity in $\operatorname{sgn}(\zeta)$ is canceled by a discontinuity in $C(\sigma,\zeta)$, and the logarithmic singularity in $\operatorname{Ci}(\sigma,\zeta)$ is cancelled by a logarithmic singularity in $S(\sigma,\zeta)$ at $\zeta=0$. It may be noted that (44) is not continuous in σ at $\sigma=0$ because we have taken the limit $\xi\to\infty$ in (42), but we shall not be interested in the case $\sigma=0$.

To evaluate the functions in (45) and (46) we assume $|\sigma|\gg 1$ so that $e^{\beta\sigma}$ is more rapidly varying than the

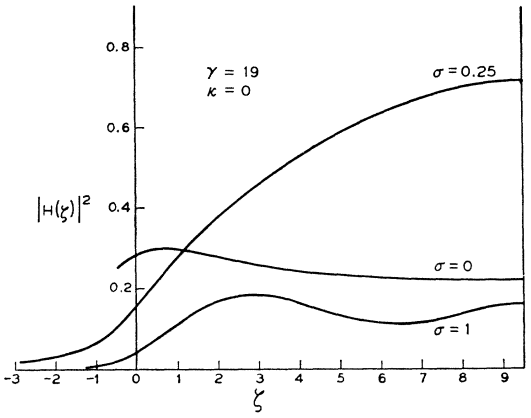

FIG. 2. Second-harmonic power as a function of focal position. The crystal surfaces are at $\zeta=0$ and $\zeta=19$, with all curves symmetric about the midpoint $\zeta=9.5$.

other factor in the integral. We may then integrate by parts to obtain

$$S(\sigma,\zeta)=\frac{1}{\sigma(1+\zeta^2)}+\frac{(1-\zeta^2)}{\sigma^2(1+\zeta^2)^2}+\frac{e^{-\sigma}}{\sigma^2\zeta^2}+\cdots, \quad (48)$$

$$C(\sigma,\zeta)=\frac{\zeta}{\sigma(1+\zeta^2)}+\frac{2\zeta}{\sigma^2(1+\zeta^2)^2}-\frac{e^{-\sigma}}{\sigma\zeta}+\cdots, \quad (49)$$

neglecting terms falling off with σ faster than σ^{-3}. Using (48), (49), and the asymptotic forms

$$\begin{aligned}\mathrm{Si}(z)&\sim\frac{\pi}{2}\,\mathrm{sgn}(z)-\frac{\cos z}{z}-\frac{\sin z}{z^2}+\cdots,\\ \mathrm{Ci}(z)&\sim\frac{\sin z}{z}-\frac{\cos z}{z^2}+\cdots,\end{aligned} \quad (50)$$

we obtain the approximations

$$\begin{aligned}R(\sigma,0,\zeta,\infty)&=2\pi e^{-\sigma}\theta(\sigma)\theta(\zeta)+\left[\frac{1}{\sigma(1+\zeta^2)}+\frac{(1-\zeta^2)}{\sigma^2(1+\zeta^2)^2}\right]\sin\sigma\zeta\\&\quad-\left[\frac{\zeta}{\sigma(1+\zeta^2)}+\frac{2\zeta}{\sigma^2(1+\zeta^2)^2}\right]\cos\sigma\zeta+\cdots, \quad (51)\end{aligned}$$

$$\begin{aligned}I(\sigma,0,\zeta,\infty)&=\left[\frac{1}{\sigma(1+\zeta^2)}+\frac{(1-\zeta^2)}{\sigma^2(1+\zeta^2)^2}\right]\cos\sigma\zeta\\&\quad+\left[\frac{\zeta}{\sigma(1+\zeta^2)}+\frac{2\zeta}{\sigma^2(1+\zeta^2)^2}\right]\sin\sigma\zeta+\cdots, \quad (52)\end{aligned}$$

valid when $|\sigma\zeta|>1$. Although we have derived this result assuming $\zeta\neq0$, we notice that the terms of order ζ^{-1} and ζ^{-2} that are present in (48), (49), and (50) have cancelled out of (51) and (52). These approximations are in fact well-behaved as $\zeta\to0$ except for the discontinuity in the first term of (51). This discontinuity is of order $e^{-\sigma}$ and therefore quite tolerable in the region of interest $|\sigma|\gg1$.

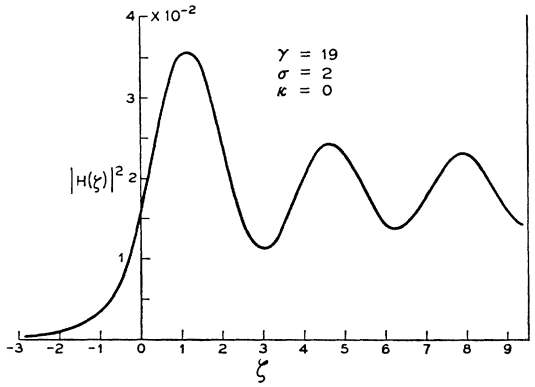

FIG. 3. Same as Fig. 2 except $\sigma=2$.

It now follows that the SHG is proportional to

$$\begin{aligned}|H(\sigma,0,\zeta,\infty)|^2&=\frac{1}{4\pi^2\sigma^2(1+\zeta^2)}+e^{-2\sigma}\theta(\sigma)\theta(\zeta)\\&\quad-\frac{e^{-\sigma}\theta(\sigma)\theta(\zeta)}{\pi\sigma(1+\zeta^2)}(\zeta\cos\sigma\zeta-\sin\sigma\zeta)+\cdots \quad (53)\end{aligned}$$

neglecting terms of order σ^{-3} and smaller. The second term will ordinarily be very small if $\sigma\gg1$, but we retain it in order to maintain the correct behavior as $\zeta\to\infty$. This is our final analytical result, valid (except for a tiny discontinuity at $\zeta=0$) for arbitrary positive or negative ζ when $|\sigma|\gg1$. We see that no structure is expected when $\zeta<0$ corresponding to the focus outside of the crystal. It is obvious that an identical discussion could be given of a large crystal with the focus approaching the exit surface and ξ replacing ζ in (53).

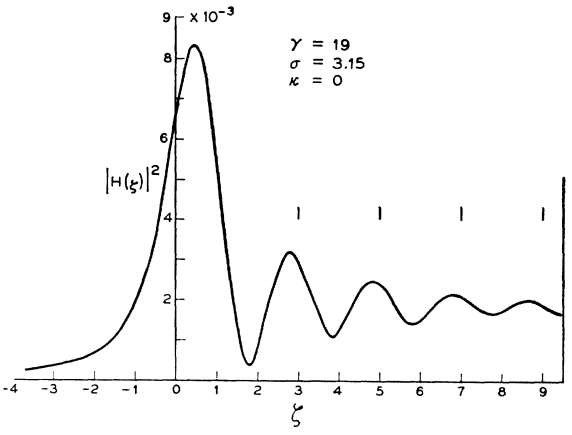

FIG. 4. Same as Fig. 2 except $\sigma=3.15$.

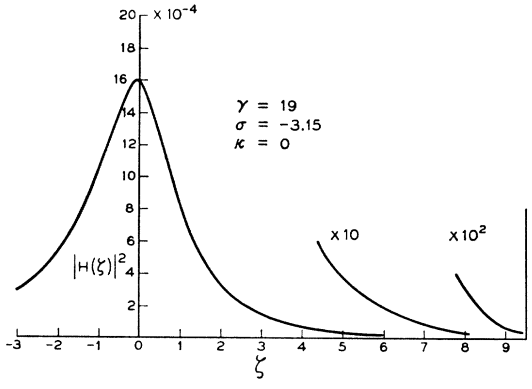

FIG. 5. Same as Fig. 2 except $\sigma=-3.15$. Notice absence of structure as compared with Fig. 4.

The main dependence of SHG on ζ is given by the first term of (53). The maximum power is obtained with $\zeta=0$ which gives

$$|H|_{\max}{}^2=1/4\pi^2\sigma^2, \tag{54}$$

and (2) becomes (no absorption)

$$P_2(\max)=4\pi KP_1{}^2/4\pi^2\delta_0\sigma^{22}, \tag{55}$$

which can be used to determine the nonlinear coefficient K from quantitative measurements of P_2 and P_1.

We now consider some representative machine calculations which illustrate the effects to be expected, and provide a check on the analytical approximation (53). We shall plot $|H(\sigma,0,\zeta,\gamma)|^2$ as a function of ζ for various values of σ and

$$\gamma=19.0. \tag{56}$$

In order to check the validity of considering an infinite crystal in (53) we present one calculation with $\gamma=1000$, which may be considered infinity. We begin with small values of σ in Fig. 2 where (53) would not be expected to hold. In the *nominal matching* case $\sigma=0$ there is very little dependence on ζ until the focus leaves the

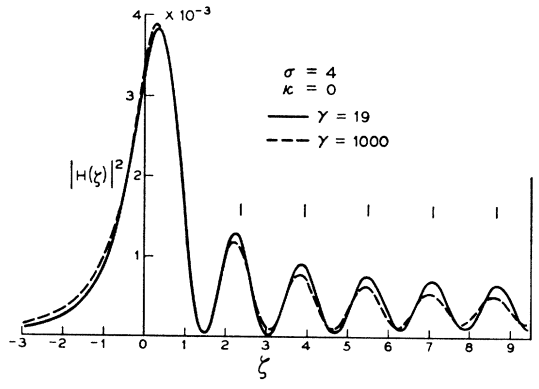

FIG. 6. Comparison of finite crystal with infinite crystal when $\sigma=4$. Infinite crystal is represented by $\gamma=1000$. Dotted curve is not symmetric about midpoint of finite crystal.

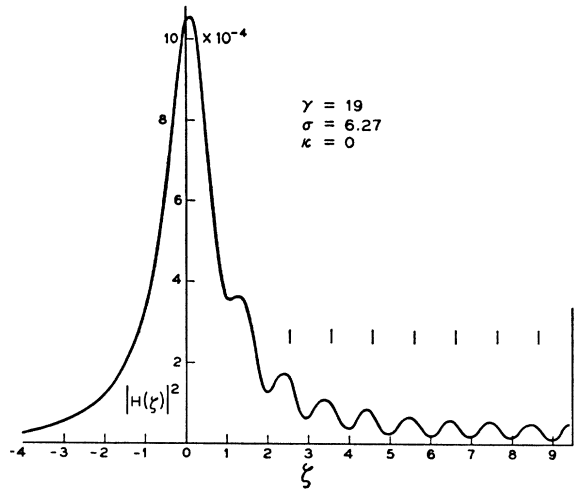

FIG. 7. Same as Fig. 2 except $\sigma=6.27$.

crystal ($\zeta<0$). The *optimum matching* case $\sigma=0.25$ corresponds to the peak of Fig. 1; in this case SHG peaks gradually in the center of the crystal as one might intuitively expect. When $\sigma=1$ there are three peaks of nearly equal width and height; since $|H|^2$ is symmetric about $\zeta=9.5$ only the region $\zeta\leq 9.5$ is shown. In Fig. 3, $\sigma=2$, there are six peaks with the peaks near the surface ($\zeta\sim 1$, $\zeta\sim 18$) considerably stronger than the rest but still appearing to be part of the same structure. Figure 4, $\sigma=3.15$, shows the surface peak much larger and wider so that it no longer appears to be part of the same structure as the other peaks. Also note the absence of structure in the region $\zeta<0$ where the focus is outside the crystal. The vertical lines indicate the positions of the maxima of $-\cos\sigma\zeta$ in this and the following figures. Figure 5, $\sigma=-3.15$,

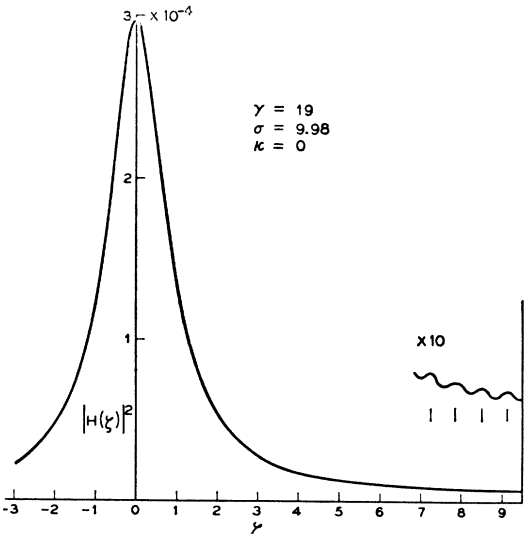

FIG. 8. Same as Fig. 2 except $\sigma=9.98$. Notice that oscillatory structure is now very weak as shown by amplified curve.

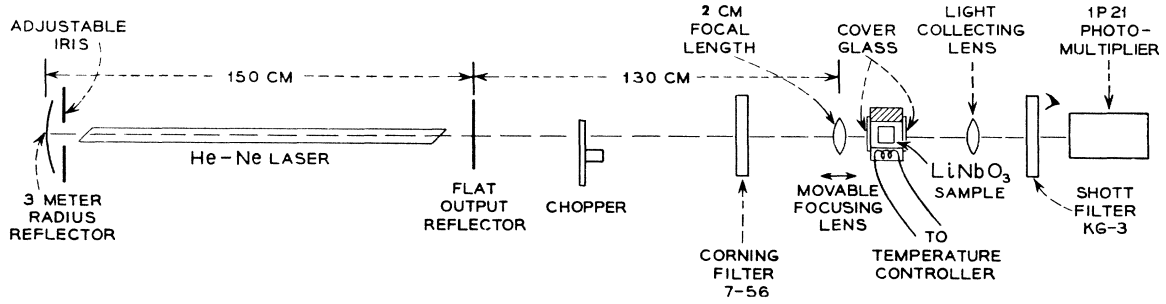

FIG. 9. Schematic layout of experiment.

shows the complete absence of oscillatory structure which theory predicts for $\sigma<0$. Figure 6, $\sigma=4$, shows a comparison of the curves for the finite crystal $\gamma=19$ and the infinite crystal ($\gamma=1000$). The difference is primarily in the phase of the oscillation at the midpoint $\zeta=9.5$ which must be a maximum or minimum in the finite crystal. Figure 7, $\sigma=6.27$, shows the further emergence of the large surface peak and the diminution of the amplitude of the oscillatory structure. The peak height 10.6×10^{-4} is in fair agreement with 6.4×10^{-4} predicted by (54). Finally Fig. 8, $\sigma=9.98$, shows the oscillations barely visible and the surface peak symmetrical about $\zeta=0$. For larger σ the curve retains this shape, which is in excellent agreement with the first term of (53). The peak 3.0×10^{-4} is in good agreement with the value 2.5×10^{-4} given by (54). A calculation at $\sigma=22.27$ gave the same shape with a peak 5.2×10^{-5} in excellent agreement with the predicted 5.1×10^{-5}. Thus the approximate theory (53) is confirmed.

V. EXPERIMENTAL APPARATUS

Experiments designed to illustrate the various phenomena discussed in the preceding sections have been performed using a 1.0798-μ He-Ne Gaussian laser beam focused into a crystal of lithium metaniobate, $LiNbO_3$.

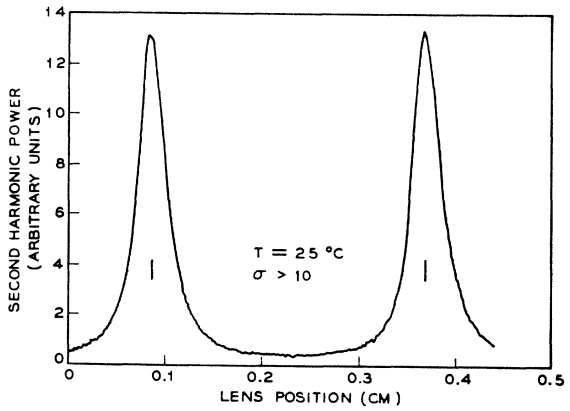

FIG. 10. Second-harmonic power as recorded on an X–Y recorder as the focusing lens is moved by a mechanical drive. The focus is at the crystal faces at the positions indicated by vertical bars.

The apparatus is indicated schematically in Fig. 9. The dc-excited laser has Brewster windows and a half-nonconfocal resonator geometry with the output, approximately 1 mW, emerging from the flat mirror. A simple iris placed near the curved mirror end of the laser cavity is adjusted so that the laser operates in the Gaussian mode. The laser resonator consists of a 3-m-radius-of-curvature mirror separated from the flat output mirror by 150 cm, while the lens is 130 cm beyond the output mirror. This geometry gives a beam radius equal to 0.0951 cm at the lens and a far-field diffraction angle equal to 4.79×10^{-4} rad.[7] The lens has a focal length of 2.0 cm so that the confocal parameter b for the beam focused into a medium of index n equals $n\times3.05\times10^{-2}$ cm. The far-field diffraction angle δ_0 of the focused beam is $4.72\times10^{-2}/n$ rad. For the present case, $n=2.23$ at 1.08 μ,[15] so b and δ_0 become 0.068 cm and 2.1×10^{-2} rad, respectively.

The $LiNbO_3$ single-domain high-optical-quality crystal[13] is 0.637 cm long and has plane-parallel opposite faces which contain the z axis—the optic axis ($LiNbO_3$ is a negative uniaxial crystal, point group $3m$). The

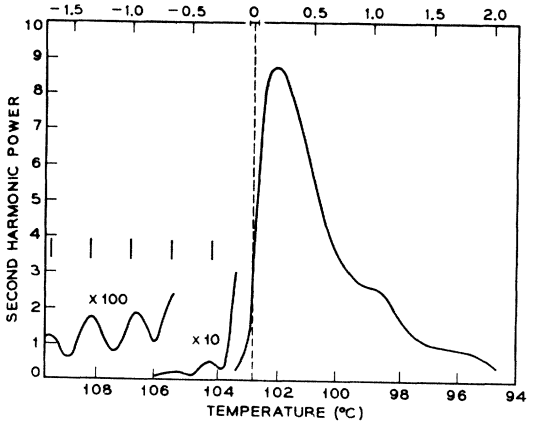

FIG. 11. Measured harmonic power as a function of crystal temperature. The σ scale at the top was calculated from independent data obtained using unfocused beams. The vertical bars mark the positions of minima for an unfocused beam. Because of the phase shift of 180° associated with the focus these bars fall at the maxima for the focused beam. This corresponds to the case $\zeta=\xi=9.4$ and therefore should agree closely with Fig. 1.

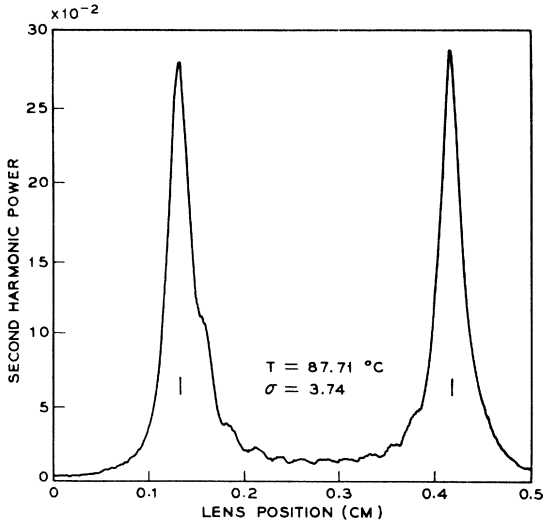

FIG. 12. Measured harmonic power as a function of focal position with same power scale as Fig. 11.

axis of the focused beam is then normal to the optic axis thereby giving rise to SHG without double refraction.[7] The SHG is via the nonlinear coefficient d_{31} and thus requires that the fundamental and harmonic rays be ordinary and extraordinary, respectively.[15] The mismatch $\Delta k=2k_1-k_2=\omega(n_1^0-n_2^e)/c$ and varies with the temperature of the crystal through the temperature-dependent refractive indices.[14] In fact, from Ref. 14 $d(n_1^0-n_2^e)/dT\approx-6\times10^{-5}$ °C^{-1} and since $n_1^0-n_2^e$ is about 0.004 at room temperature,[15] the mismatch can be easily varied via the crystal temperature from $\Delta k\gg\pi/l$ through $\Delta k=0$ to $-\Delta k\gg\pi/l$. The crystal is mounted in a large silver block with electrical heaters thus providing a means of varying Δk thermally. The temperature of the silver block is controlled to about ±0.05°C.

The lens can be moved at various preselected speeds with respect to the sample by means of a mechanical drive. While the lens is being moved, the second harmonic output is recorded on an X-Y recorder.

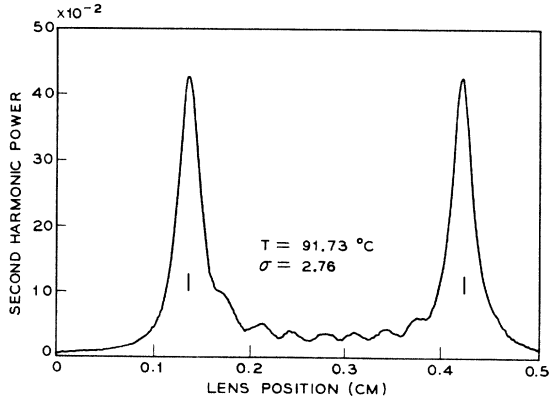

FIG. 13. Measured harmonic power on the power scale of Fig. 11.

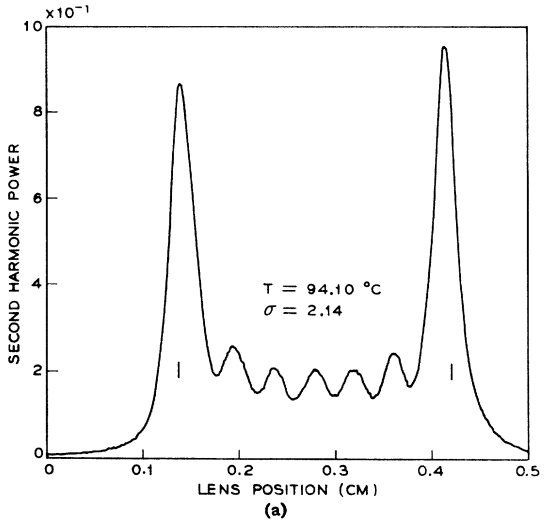

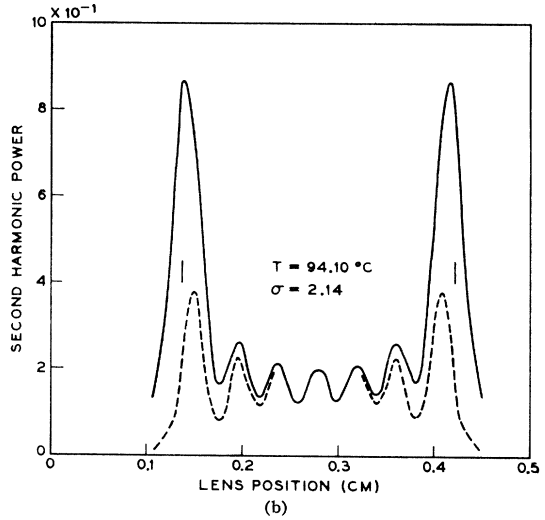

FIG. 14. (a) Measured harmonic power on scale of Fig. 11. (b) Theoretical fit to (a) using $\sigma=2.25$ and adding enough of the first term of (53) to give the correct peak height. The contribution of $|H(2.25,0,\zeta,19)|^2$ is shown dashed.

Phase-sensitive detection is used for the second harmonic. A typical plot obtained at room temperature is reproduced in Fig. 10. For this case, where $\sigma>10$, two large second harmonic peaks are obtained and found to coincide exactly with the crystal surfaces. The experimental data in Fig. 10 are seen to be in qualitative agreement with the theoretical plot shown in Fig. 8. Plots of this sort have been obtained as a function of crystal temperature as will be described.

5. EXPERIMENTAL RESULTS

The data in Fig. 11 show the second harmonic intensity as a function of temperature with the lens focused in the center of the sample. (The center of the sample is easily located with the aid of a second-harmonic intensity versus lens position plot like that

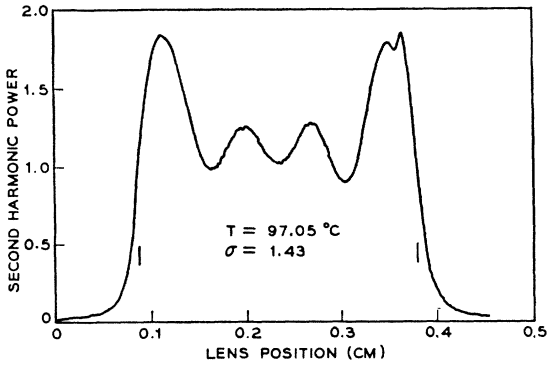

FIG. 15. Measured harmonic power on scale of Fig. 11.

shown in Fig. 10.) Unfocused beam studies with the same crystal described above show that $\Delta k=0$ at $T\equiv T_0=102.75°C\pm0.13°C$,[16] and other unfocused beam data[17] give $d\Delta k/dT=-7.35$ cm^{-1} °C^{-1} in the vicinity of T_0. These data for the unfocused situation were then used to calculate $\sigma=\Delta kb/2$ as a function of temperature. The σ scale at the top of the figure was obtained in this manner. The calculated value of $\zeta=\xi$ for the experimental situation is 9.4 so that these results can be compared with Fig. 1.

It is evident that the experimental data exhibit all the qualitative features given by the theory. The short vertical lines shown in Fig. 11 for $\sigma<0$ are the positions of the second harmonic *minima* calculated for the plane-wave case from unfocused beam data.[17] As noted in (21) and (22), and shown in Fig. 1, these lines should mark intensity *maxima* in the case of a focused beam. It is seen that in agreement with theory, the experimental maxima in Fig. 11 for $\sigma<0$ do occur

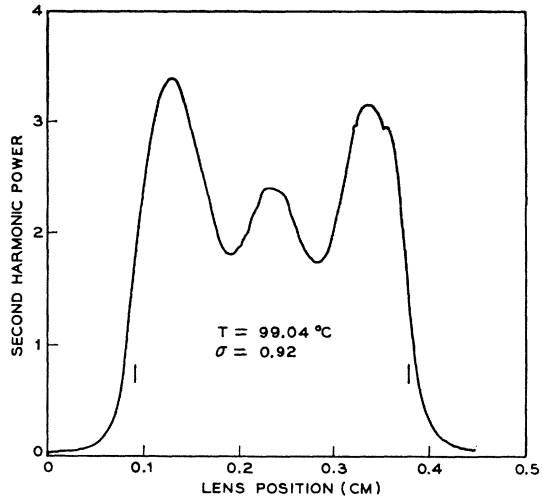

FIG. 16. Measured harmonic power on scale of Fig. 11.

[16] The value of T_0 has been found to vary by more than 100°C from one $LiNbO_3$ boule to another for reasons which are at present not understood.

[17] R. C. Miller (unpublished data).

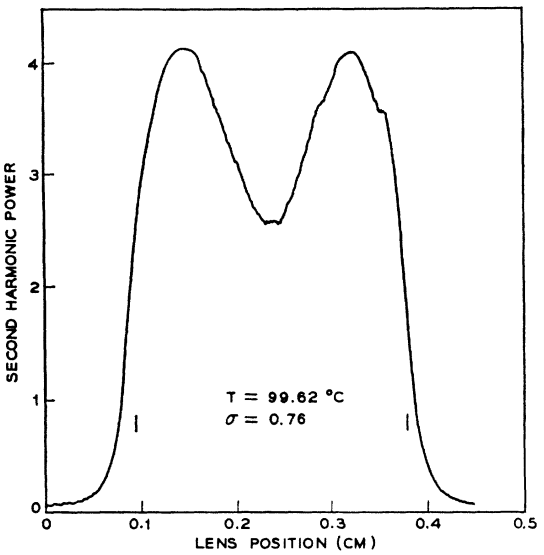

FIG. 17. Measured harmonic power on scale of Fig. 11.

at the positions of the short vertical lines. The failure of the experimental minima for $\sigma<0$ to go to zero as predicted by the theory is believed to be due to small temperature gradients in the crystal and a small background second harmonic arising from the 1.15-μ He-Ne laser line also present in the focused beam. The contribution of the 1.15-μ second harmonic is of the order of 0.1% of the maximum 1.08-μ harmonic shown in Fig. 11. Therefore, only for $\sigma<0$ and $\gtrsim3$ will the 1.15-μ contribution be significant when the focus is in the center of the crystal. Although the presence of the 1.15-μ line in the laser beam makes a detailed quantitative comparison between theory and experiment somewhat uncertain for the two σ regions mentioned above, it can be taken into account in a simple and satisfactory way.

Figures 12 through 21 show the second harmonic

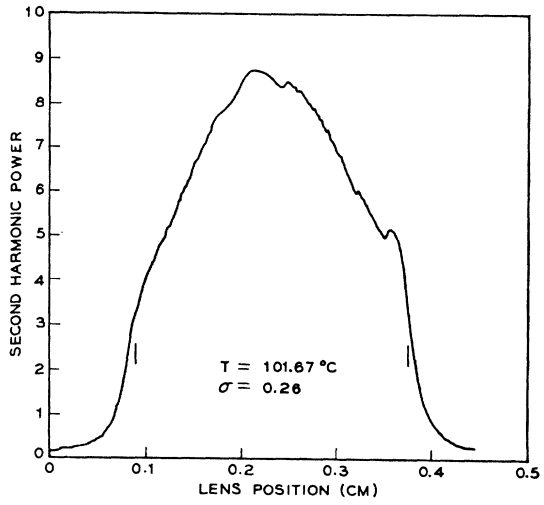

FIG. 18. Measured harmonic power on scale of Fig. 11.

intensity as a function of lens position for various representative temperatures in the vicinity of T_0. In each case the figures include the temperature, the calculated value of σ, the positions of the faces of the crystal, and an intensity scale the same as that in Fig. 11. For $\sigma=3.74$, 2.76, and -1.35, the intensity scales have been adjusted for the focus in the center of the crystal to compensate for the 1.15-μ second harmonic contribution; however, no attempt has been made to subtract this contribution as a background. With the scales adjusted in this manner, the intensities for the focus in the center of the crystal can be compared with Fig. 11, and after a change of scale, with Fig. 1.

The comparison with Fig. 1 shows that the experimental intensities observed with the focus in the center of the crystal are in good agreement with the theory.

Figure 14(b) shows a theoretical plot considered to be in excellent agreement with the experimental data of Fig. 14(a). The theoretical plot includes contributions from both the 1.08-μ ($\sigma=2.14$) and the 1.15-μ ($\sigma\approx 50$) harmonics. The dashed curve shows the 1.08-μ harmonic calculated for $\sigma=2.25$, while the solid curve shows the sum of the above contribution and a "universal curve" (valid for $\sigma>10$) of the form given by the first term of Eq. (53) to represent the 1.15-μ harmonic contribution. The shape of the universal curve is independent of σ. The relative magnitudes of the two harmonics and the value of σ for the 1.08-μ line were varied to obtain the theoretical fit shown. The 1.15-μ harmonic is only significant for the beam focused away from the center of the crystal. While other values of σ for the 1.08-μ line slightly different from 2.25 do not, in general, result in such good agreement between theory and experiment, a theoretical plot with $\sigma=2.40$ and a suitable contribution from the universal curve also appears to give a satisfactory fit. However, when the uncertainties in T_0 and $d\Delta k/dT$ are taken into account, the value of $\sigma=2.14$ calculated from the unfocused beam data[17] is considered to be in agreement with $\sigma=2.24$, but not with $\sigma=2.40$. Hence the "theoretical fit" with $\sigma=2.40$ has been rejected.

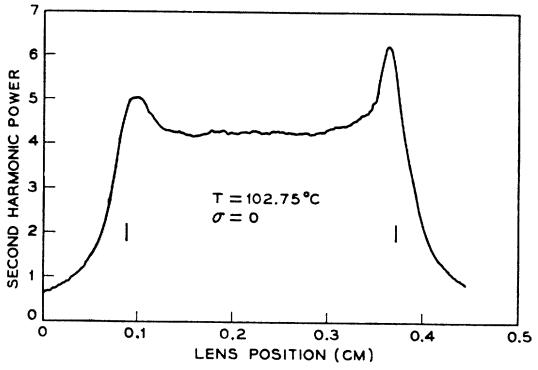

FIG. 19. Measured harmonic power in nominal matching case $\sigma=0$. This should agree with $\sigma=0$ curve of Fig. 2.

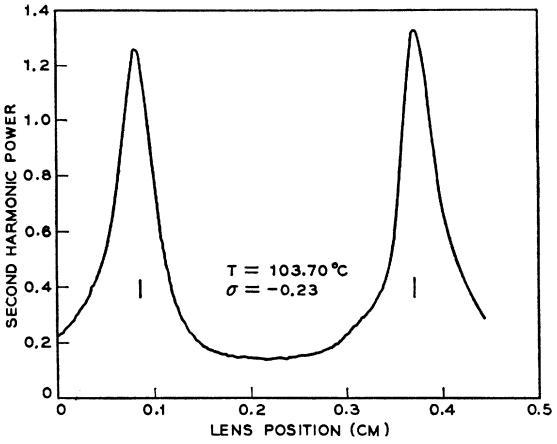

FIG. 20. Measured harmonic power for negative $\sigma=-0.23$. Notice absence of structure.

In the theoretical section it has been shown that the coherence length l_c can be obtained from the data when oscillations in the intensity with lens position occur. However, inspection of the theoretical plots shows that the period of the oscillation is not exactly equal to l_c when there are few minima (Fig. 2) or when the amplitudes of the minima vary significantly with distance (Fig. 4). Both of these effects can give an l_c determined from the curve too small by about 10%. Calculation of l_c's from the experimental data yields values roughly 5% smaller than those deduced from the temperature dependence of Δk. This result is not surprising in view of the comments above and the 5% or so uncertainty in $\Delta k(T)$. It should be noted that in agreement with theory, no intensity oscillations with lens position are observed for $\sigma<0$.

The small-intensity peaks observed with the lens focused near the front of the crystal for small positive

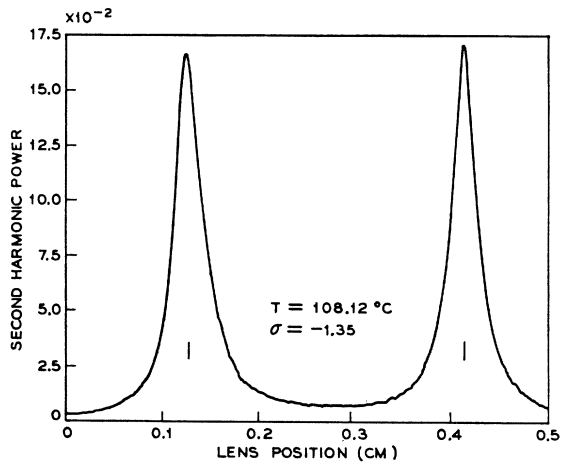

FIG. 21. Measured harmonic power for $\sigma=-1.35$.

values of σ are not understood. Other data not shown also in some cases exhibit a similar peak with the focus near the back of the crystal.

To demonstrate the usefulness of the focused beam technique for determining nonlinear coefficients under nonphase-matched conditions, the ratio of d_{33}/d_{31} for $LiNbO_3$ has been obtained with the 1.15-μ He-Ne line. Prior to the present measurement, the ratio was known only for the 1.06-μ pulsed Nd laser in which case d_{33}/d_{31} was reported to be 9.0 ± 3.0.[15] In the present experiment, the second-harmonic intensity versus lens position was determined for the second harmonic due to each of the two coefficients. The only significant difference in the experimental arrangement between the two measurements was that imposed by the polarization requirements of the SHG process. In particular, for d_{31} the fundamental and harmonic are ordinary and extraordinary waves, respectively, while for d_{33} both waves are extraordinary waves. Since the laser polarization was not changed, these polarization requirements necessitated a rotation of the sample by 90° about the beam axis in going from d_{31} to d_{33}. From Eqs. (3), (8), (10), and (55), one finds

$$(P_2\,\max)_{33}/(P_2\,\max)_{31}=\left[\frac{(P_1)_{33}d_{33}(l_c)_{33}}{(P_1)_{31}d_{31}(l_c)_{31}}\right]^2 \quad (57)$$

which can then be used to determine d_{33}/d_{31}. The coherence lengths are determined from the known indices.[15] It is found that $d_{33}/d_{31}=6.0\pm1.0$ for the 1.15-μ line which is to be preferred to the previous measurement. On a scale where $d_{36}\equiv1.00$ for KH_2PO_4, $d_{31}=10.6\pm1.0$,[15] so that $d_{33}=64\pm16$ on this scale. It is unfortunate that the second-order nonlinear optical processes are such that this large coefficient cannot be phase-matched.

This method for determining nonlinear coefficients has some advantages over other techniques.[4,18,19] Several of these advantages are: it is fast, it can be used with a small sample, it requires only one moderately good surface on the sample, and it is not restricted to phase-matchable materials. One disadvantage is that this technique requires knowledge of the coherence length. Therefore other independent measurements will usually be necessary to determine l_c since it cannot be obtained from a second-harmonic-intensity–versus–lens-position plot for $l_c\ll b$ which will usually be the case.

6. SUMMARY

The effects of moving the position of the focus in SHG have been described theoretically and observed experimentally. The effects depend greatly upon the coherence length, and are particularly interesting when the mismatch parameter σ defined by (5) lies in the range $1<\sigma<10$. This range is illustrated in Figs. 2–4, 6–8. When $\sigma<0$ or $\sigma>10$ the fine structure sensitive to the coherence length is absent or very weak as shown in Figs. 5 and 8. With the focus at the center of the crystal the dependence of SHG on mismatch is shown in Fig. 1. These curves were calculated by high-speed computer directly from (1) and (2) derived previously.[1] As an aid in understanding the dependence on focal position a new asymptotic approximation not previously given has been developed for the nonmatching case $|\sigma|\gg1$. This approximation (53) is well behaved at all positions of the focus and accounts satisfactorily for the peak of intensity at the surface and the fine structure. The neglect of double refraction and absorption is valid if the crystal length is less than the aperture length[7] and less than the absorption length for the laser or the harmonic.

Experiments are reported using a crystal of $LiNbO_3$ and a He-Ne gas laser. The crystal was oriented to eliminate double refraction, and the coherence length could be controlled through the crystal temperature. The SHG as a function of temperature with the focus in the center of the crystal is given in Fig. 11, which is in satisfactory agreement with the calculated Fig. 1. The dependence on focal position for various values of σ is shown in Figs. 12–21. The same (arbitrary) power scale is used in Figs. 11–21. The peaking at the surfaces, the fine structure, and the absence of fine structure for $\sigma<0$ and $\sigma>10$ are found in qualitative agreement with theory. A satisfactory quantitative comparison with theory for the case $\sigma=2.14$ is shown in Figs. 14(a) and 14(b). To obtain agreement an appropriate amount of the first term of (53) representing the harmonic of the 1.15-μ laser line was added to the calculated curve for $\sigma=2.25$. Extra lines can easily be taken into account in this manner if they have $|\sigma|\geq10$, since then the shape of the curve is a universal function independent of σ and given by the first term of (53). Finally the 1.15-μ laser line having $\sigma\sim50$ was used to measure the ratio d_{33}/d_{31} for $LiNbO_3$ by observing the peaks at the surface produced by the extraordinary and ordinary components of the laser beam.

We conclude that the theory of SHG in regard to the dependence on coherence length and position of the focus is in satisfactory agreement with experiment. Focused beams under nonmatching conditions are convenient for quantitative measurements of nonlinear optical coefficients providing the coherence length is known.

ACKNOWLEDGMENTS

The authors would like to thank Dr. K. Nassau who grew and generously provided the fine $LiNbO_3$ crystals, and A. Savage who made numerous important contributions to the experimental phases of this research.

[18] J. Ducuing and N. Bloembergen, Phys. Rev. Letters **10**, 474 (1963).

[19] A. Ashkin, G. D. Boyd, and J. M. Dziedzic, Phys. Rev. Letters **11**, 14 (1963).